Hindawi
Journal of Nanomaterials
Volume 2018, Article ID 9721730, 9 pages
https://doi.org/10.1155/2018/9721730

Research Article

Preparation and Characterization of TATB/VitonA Nanocomposites

Wenzheng Xu, Zhaoying Pang, Jingyu Wang, Chao Ping, Jie Wang, and Jinyu Peng

School of Environment and Safety Engineering, North University of China, Taiyuan, 030051 Shanxi, China

Correspondence should be addressed to Wenzheng Xu; xuwznuc@126.com

Received 20 May 2018; Revised 5 September 2018; Accepted 18 September 2018; Published 23 December 2018

Academic Editor: Jean M. Greneche

Nano-TATB particles were prepared by an ultrasonic-assisted spray method. Molecular dynamics simulation was used to select the best binder—VitonA. Then, using VitonA as a binder, TATB/VitonA nanocomposites were prepared by a compressed air spray evaporation method and the formation mechanism of TATB/VitonA nanocomposites was proposed. Meanwhile, the crystal morphology, particle size, crystal structure, thermal decomposition properties, and impact sensitivity properties of the raw materials of TATB, the prepared nano-TATB particles, and the TATB/VitonA nanocomposites were characterized by a scanning electron microscope (SEM), laser particle size analyzer (LPSA), X-ray diffractometer (XRD), differential scanning calorimeter (DSC), and impact sensitivity instrument. The detonation performances of TATB/VitonA were calculated by the EXPLO5 program. The results indicated that the size of TATB/VitonA nanocomposites was 0.5–1 μm. The results also indicated that TATB/VitonA nanocomposites were composed of many nano-TATB particles (40–60 nm). The crystal structure of TATB/VitonA nanoparticles was not changed. The activation energy of TATB/VitonA nanocomposites was higher than nano-TATB particles by 42.62 kJ·mol^{-1}, and the characteristic drop of the proportion of TATB/VitonA nanocomposites was higher than nano-TATB particles by 13.8 cm. The thermal stability of TATB/VitonA nanocomposites was higher, while their mechanical sensitivities were lower, which showed potential for sustainable use in the field of energetic materials.

1. Introduction

1,3,5-Triamino-2,4,6-trinitrobenzene (TATB) is a kind of heat-resistant explosive with low detonation sensitivity which is very stable and insensitive. It is often used in high-speed missile warheads due to its safety during handling [1–3]. TATB hybrid explosives are particularly attractive in modern weapons, astronautics, and nuclear weapons because such explosives can meet the safety requirements arising from high temperatures and accidents. The possibility of using TATB as an insensitive blasting material is investigated by the U.S. Department of Defense (DoD) because of the safety features of TATB and its greater explosive power compared to equivalent TNTs [4, 5]. The two formulations of the LX-17 developed by the Lawrence Livermore National Laboratory and the PBX-9502 developed by the Los Alamos National Laboratory, all of which are TATB-based plastic adhesive explosives, have been established as insensitive explosives for nuclear weapons by the U.S. Department of Energy (DoE) [6, 7]. These two formulations of TATB are based on plastic bonded explosives. TATB is considered as the most important insensitive high explosive (IHE). Therefore, TATB-based PBX was applied to modern nuclear weapons by DoD and DoE.

At present, the main methods for preparing insensitive high explosives are as follows: ultrafining [8], cocrystal coating [9], and surface coating [10]. Ultrafining and surface coating are considered to be the most effective and convenient methods. TATB nanoparticles with a particle size of about 60 nm and particle surface area of 22 m^2/g were prepared by Yang et al. [11]. It could be concluded that nano-TATB particles will provide a higher surface energy and higher explosive energy. In 2012, Yang et al. [12] prepared an ultrafine TATB by the solvent and nonsolvent recrystallization method. The ellipsoid and spherical TATB particles with a size range of 30 to 50 nm were prepared

from TATB raw materials with 0.095% (mass percentage) of ionic surfactant (S) as additive using a spraying device. The spherical TATB particles with a particle diameter of 50 nm and a narrow distribution were also prepared when using 0.014% nonionic surfactant (P) as additives. In 2017, nano-TATB with an average particle size of 58.1 nm was prepared by a high-energy mechanical milling method by Song et al. [13]. The morphology of nano-TATB was characterized by a scanning electron microscope (SEM), and the particle size distribution was calculated. A solvent mixed with 3-ethyl-1-methylimidazolium acetate-dimethyl sulfone (EMImOAc-DMSO) was used by Gee et al. [14] to obtain TATB through recrystallization. The solvent was heated to 100°C to obtain a red blood solution, and water was added to complete precipitation. The TATB crystal obtained was irregular and had a rough surface with a particle size distribution of 0.5–5 μm.

One of the most effective ways to reduce sensitivity is to coat the surface of the high explosive. It is possible to control the forming, mechanical, and thermal decomposition properties of the composites by controlling the content of the binder. The proportion of the binder required in PBX is usually 2 to 10%. The content of the binder has a significant influence on the explosive and mechanical properties of PBX [7, 15, 16]. In recent years, spray drying was used by many researchers to coat the surface of ultrafine explosives with a small amount of binder, which could significantly reduce the sensitivity of the high explosives [17–20]. Yang et al. [21] prepared a compact TATB/CL-20 core-shell structure by adding a polymer binder. The result showed that 100% coverage of the core-shell structure was obtained. 1,3,5-Trichloro-2,4,6-trinitrobenzene (TCTNB) was added to an HMX-toluene solution, and it was aminated so that the HMX crystal was in situ coated by TATB generated by Nandi [22]. The coating layer on the surface of the HMX crystal made using an acoustic chemical method was more uniform than that made using the conventional method. Hybrid graphene/multiwalled carbon nanotubes were selected by Lin et al. [23] as a filler to improve the nonlinear viscoelastic properties of TATB-based PBX. The morphology, mechanical properties, and creep behavior of TATB-based PBX were investigated.

In this paper, nano-TATB was prepared by an ultrasonic-assisted spray method, and then TATB/VitonA nanocomposite microsphere-based nano-TATB was prepared by the compressed air spray evaporation method. The formation process of TATB/VitonA composite particles was detailed, researched, and analyzed.

2. Experimental Parts

2.1. Materials. Raw TATB was produced by Gansu Yinguang Chemical Industrial Company. A copolymer of vinylidene fluoride and hexafluoropropylene (VitonA) was produced by Sichuan Chenguang Chemical Company. Dimethyl sulfoxide (DMSO) and ethyl acetate were purchased from Tianjin Fuchen Chemical Reagent Company. 3-Ethyl-1-methylimidazolium acetate (EMImOAc) was purchased from Shanghai Cheng Jie Chemical Company Ltd.

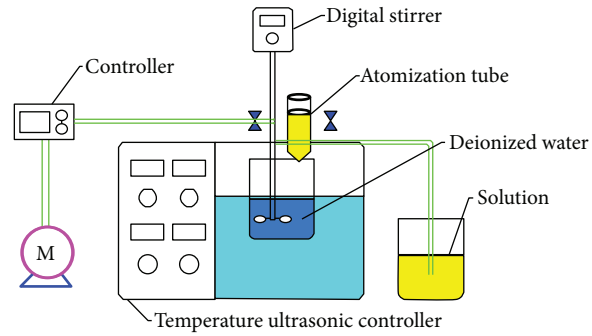

Figure 1: Ultrasonic-assisted spray refinement experimental device.

2.2. Preparation of Nano-TATB. Nano-TATB was prepared by the ultrasound-assisted spray method. The experimental device is shown in Figure 1. The experimental procedure is as follows: (i) Firstly, 10 g of raw TATB is dispersed in a mixed solvent of 900 ml of DMSO and 50 g of EMImOAc. (ii) Secondly, the mixed solvent is heated to 90°C until the raw TATB is completely dissolved in an ultrasonic system with a 40 kHz frequency and 600 W output power (JETAN Ultrasonic Cleaner JP-100S, Shenzhen, China). (iii) Thirdly, the ultrasonic controller and digital stirrer are turned on and the TATB solution is sprayed into the beaker through the atomization tube to form a suspension. (iv) Finally, the yellow suspension is washed, filtered, and vacuum freeze-dried to obtain nano-TATB particles.

2.3. Preparation of TATB/VitonA Nanocomposites. The experimental device for preparing TATB/VitonA nanocomposites by compressed air spray evaporation is shown in Figure 2. The experimental procedure is as follows: (i) Firstly, 0.3 g of VitonA is dissolved in 20 ml of ethyl acetate and then VitonA is completely dissolved to form a transparent solution. (ii) Secondly, 9.7 g of nano-TATB is added to 20 ml of ethyl acetate, then the solution of the binder in (i) is also added and stirred until the yellow suspension is finally obtained. (iii) Finally, the suspension liquid is poured into an atomizing device. When driven by a high-speed compressed gas generated by an air compressor, the liquid is sprayed into a tube with a circulating heating device. After ethyl acetate is evaporated by a heating device, TATB/VitonA nanocomposites are obtained.

2.4. Characterization. The crystal morphologies of nano-TATB and TATB/VitonA nanocomposites were characterized by using a field emission scanning electron microscope (SEM, TESCAN MIRA3 LMH, TESCAN, Czech Republic). The particle size was measured by a laser particle size analyzer (LPSA, NanoBrook 90Plus, Brookhaven Instruments Corporation, USA). X-ray diffraction (XRD, DX-2700, Dandong Haoyuan Corporation, Liaoning, China) was used to analyze the crystal form of the samples at a voltage of 40 kV and a current of 30 mA. The thermal decomposition characteristics of the samples were measured on a differential scanning calorimeter (DSC, DSC 131, Setaram Corporation, France). The test conditions are as follows: nitrogen atmosphere with a flow rate of 30 ml/min; sample quality of

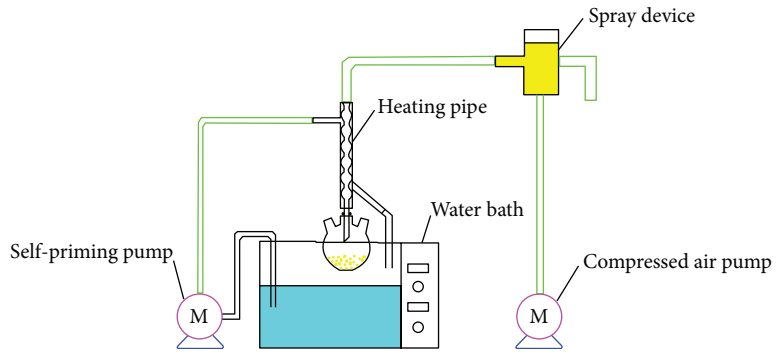

Figure 2: Experimental device for preparing TATB/VitonA noncomposites.

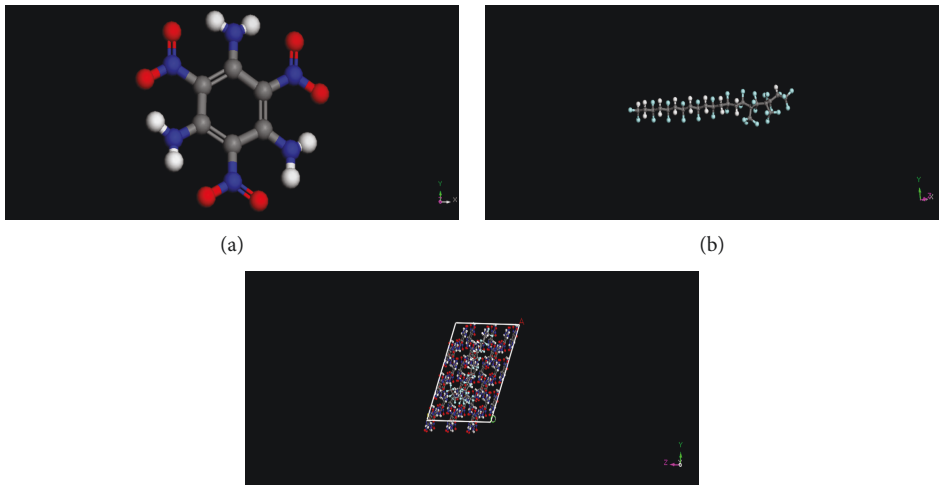

Figure 3: TATB (a) and VitonA (b) molecular structure models and TATB/VitonA (c) molecular equilibrium structure diagram.

0.7 mg; Al_2O_3 powder was used as reference material; and β heating rates were 5, 10, 15, and 20°C/min, respectively. The impact sensitivity was tested by a homemade type 12 drop hammer. The testing conditions are as follows: drop weight, 10.000 ± 0.002 kg; sample mass, 35 ± 1 mg; temperature, 10–35°C; and relative humidity, ≤80%. The results were based on tests on both sides of the 50% probability level using an up-and-down method. Each sample was tested 25 times to obtain H_{50} (the H_{50} value represents the falling height of the explosive when the probability of explosion is 50%).

3. Result and Discussion

3.1. Molecular Dynamics Simulation. Molecular dynamics simulation was used to simulate TATB/VitonA. The mass fraction of the binder was set at 3%. The molecular structure models of TATB and VitonA and the molecular equilibrium diagram of TATB/VitonA are shown in Figure 3. The density of the model was close to the theoretical density of TATB when the polymer binder was placed in the vacuum layer of the TATB supercell, and the supercell space was compressed. Then, the model was optimized to reduce the energy of the system. The TATB/VitonA system was simulated by an NVT system under a COMPASS force field. The curve of

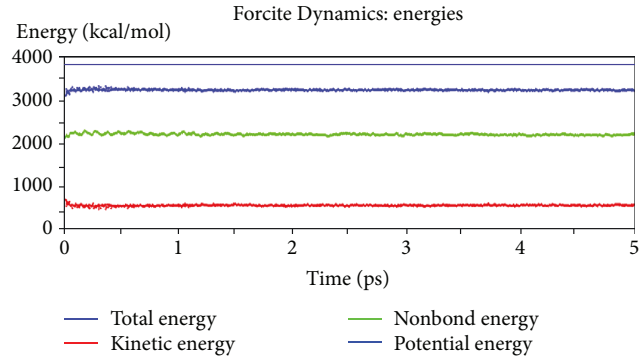

Figure 4: TATB/VitonA energy curve over time.

energy and temperature over time for TATB/VitonA are shown in Figures 4 and 5. Under the stable equilibrium structure of the system, the total energy of the system was used to calculate the binding energy. The average interaction energy ΔE of the polymer binder on the surface of the TATB crystal can be expressed as:

$$\Delta E = -\left(E_{\text{total}} - E_{\text{poly}} - E_{\text{TATB}}\right), \quad (1)$$

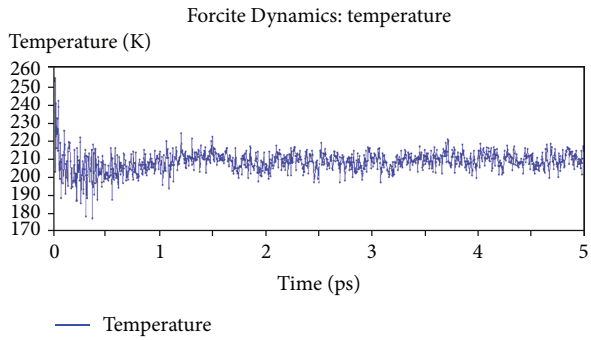

Figure 5: TATB/VitonA temperature curve over time.

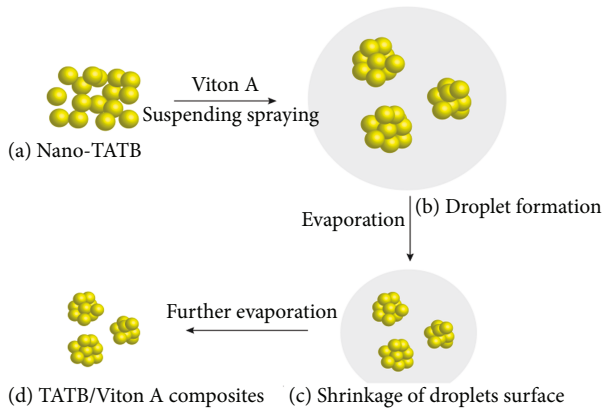

Figure 6: Schematic diagram of the mechanism of TATB/VitonA nanocomposites formed by compressed air spray evaporation.

where E_{total} is the average total energy of TATB/VitonA nanocomposites (561.45 kJ/mol), E_{poly} is the average singlet energy of the polymer binder VitonA (−689.79 kJ/mol), and E_{TATB} is the average singlet energy of TATB (3392.53 kJ/mol).

The binding energy ΔE of the TATB/VitonA system was 2141.29 kJ/mol. Since the binding energy could be used to characterize the compatibility of TATB with the binder, it was calculated that the compatibility of TATB and VitonA was better, so VitonA was selected as the binder.

3.2. Formation Mechanism of TATB/VitonA Nanocomposites. As shown in Figure 6, the formation mechanism of the TATB/VitonA nanocomposite was proposed by the compressed air spray evaporation method. Firstly, nano-TATB particles were prepared by ultrasound-assisted spray (Figure 6(a)). Then, nano-TATB and the binder solution (VitonA) were mixed and added into a compressed air atomizing device. Through the small nozzle, compressed air was used to form a high-speed air stream to generate a negative pressure to spray the mixed solution together onto the fogging baffle. In the high-speed impact to the surrounding splash, the droplets became foggy particles which were ejected from the spray outlet (Figure 6(b)). The foggy particles were heated by the circulating heating device and the solvent was evaporated. Finally TATB/VitonA nanocomposites with a uniform and dense spherical shape were formed (Figure 6(d)).

3.3. Morphology and Size Characterization. The morphology and size of the samples were probed by SEM and LPSA, and the results are illustrated in Figures 7 and 8. Figures 7(a) and 7(b) show images of raw and nano-TATB. The raw TATB particles were larger with an irregular shape, and the average particle size distribution was about 25 μm. There were no obvious edges and corners on the surface of the particles, and particles were relatively smooth. The nano-TATB particles had a regular spherical shape without obvious defects on the smooth surface and had a narrow crystal size distribution of 40–60 nm. Images of TATB/VitonA nanocomposites at different magnifications are shown in Figures 7(c)–7(e). The morphology of the TATB/VitonA nanocomposites was spherical with a smoother surface and a narrower particle size distribution (Figures 7(c) and 7(d)). The particle size of the TATB/VitonA nanocomposites was about 0.5–1 μm (Figures 7(e) and 7(f)), and many nano-TATB particles were bonded together on the surfaces of the composites. The particle size distribution of nano-TATB is shown in Figure 8. It is obvious that the median diameter of nano-TATB is 45.2 nm and the average particle size is 50 nm, indicating a relatively narrow particle size distribution.

3.4. XRD Analysis. The XRD patterns of the raw TATB, nano-TATB, and TATB/VitonA nanocomposites are shown in Figure 9. The diffraction angle of the raw TATB is basically conformed to the nano-TATB (28.297° and 28.366°). The diffraction peak intensity of raw TATB (Figure 9(a)) particles was 4539, and the half width was 0.435°. The diffraction peak intensity of nano-TATB (Figure 9(b)) was 2736, and the half width was 0.615°. It showed that the refinement process did not change the crystal structure of TATB, but the peak intensity was weaker and the peak shape was broader, which correspond to the characteristic of the X-ray diffraction of typical nanoparticles. The diffraction peak intensity of the TATB/VitonA nanocomposites (Figure 9(c)) was obviously reduced, and the peak shape was broadened. The position of the diffraction peak of TATB/VitonA nanocomposites was matched to TATB. There was no new diffraction peak, which would indicate that the spray evaporation coating process did not change the crystal structure of the material.

3.5. Analysis of Thermal Stability. The thermal analyses of the raw TATB, nano-TATB, and TATB/VitonA nanocomposites were carried out at the β heating rates of 5, 10, 15, and 20°C/min, respectively. The results of DSC analysis are shown in Figure 10. For different heating rates, the decomposition peak temperatures of raw TATB and nano-TATB were increased with the increase of the heating rate (Figures 10(a) and 10(b)). Under the same heating rate, the peak temperature of decomposition of nano-TATB was about 10°C which was lower than that of the raw TATB. This was due to the fact that when the explosive particles were reduced, the progress of heat transfer would be accelerated, resulting in faster thermal reaction rate, worse thermal stability, and lower thermal decomposition temperature. The exothermic peak temperatures of TATB/VitonA nanocomposites were 360.32°C, 370.21°C, 374.97°C, and 379.83°C, respectively. It was obvious that the exothermic peak temperatures were increased

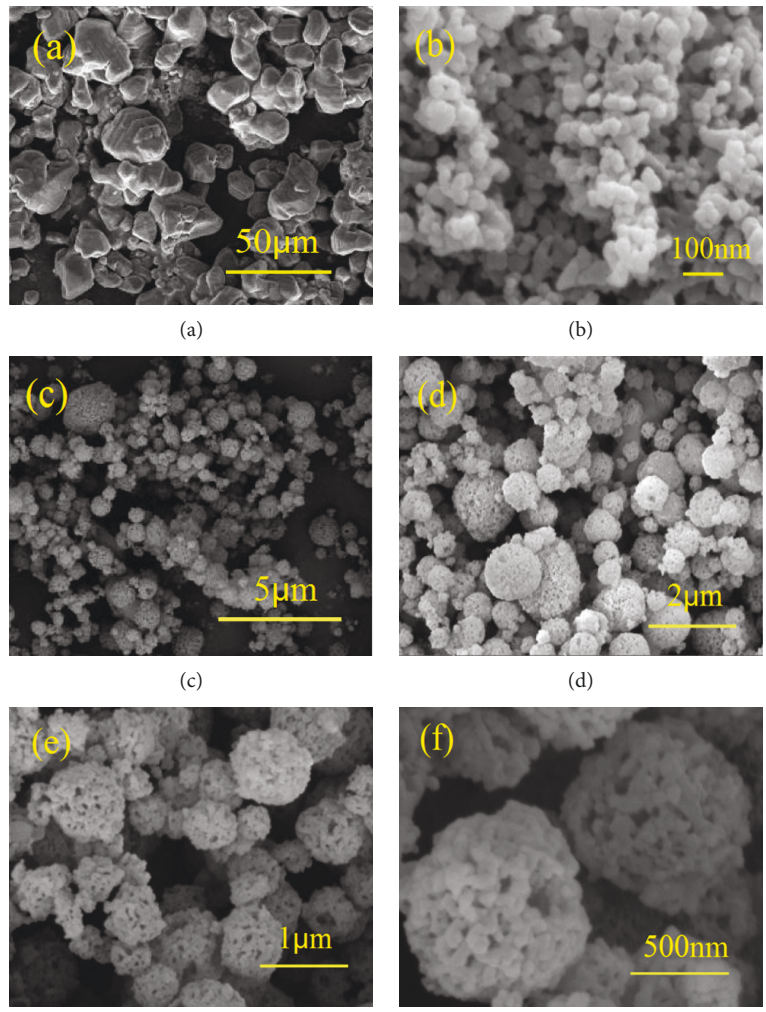

FIGURE 7: Raw TATB (a), nano-TATB (b), and TATB/VitonA nanocomposites (c–f) at different magnifications.

Sample ID	TATB
Operator ID	H
Elapsed time	00:02:00
Median diam.	45.2 nm
Mean diam.	50.0 nm
Polydispersity	0.243
GSD	1.594

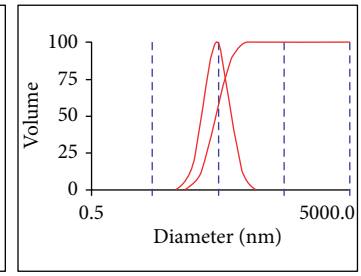

d (nm)	G (d)	C (d)	d (nm)	G (d)	C (d)	d (nm)	G (d)	C (d)
21.6	26	5	40.3	97	40	61.1	80	75
25.4	44	10	42.7	99	45	65.9	70	80
28.4	58	15	45.2	100	50	71.9	58	85
31.0	70	20	47.8	99	55	80.3	44	90
33.4	80	25	50.6	97	60	94.5	26	95
35.7	87	30	54	92	66			
38.0	93	35	57.2	87	70			

FIGURE 8: Particle size distribution of nano-TATB.

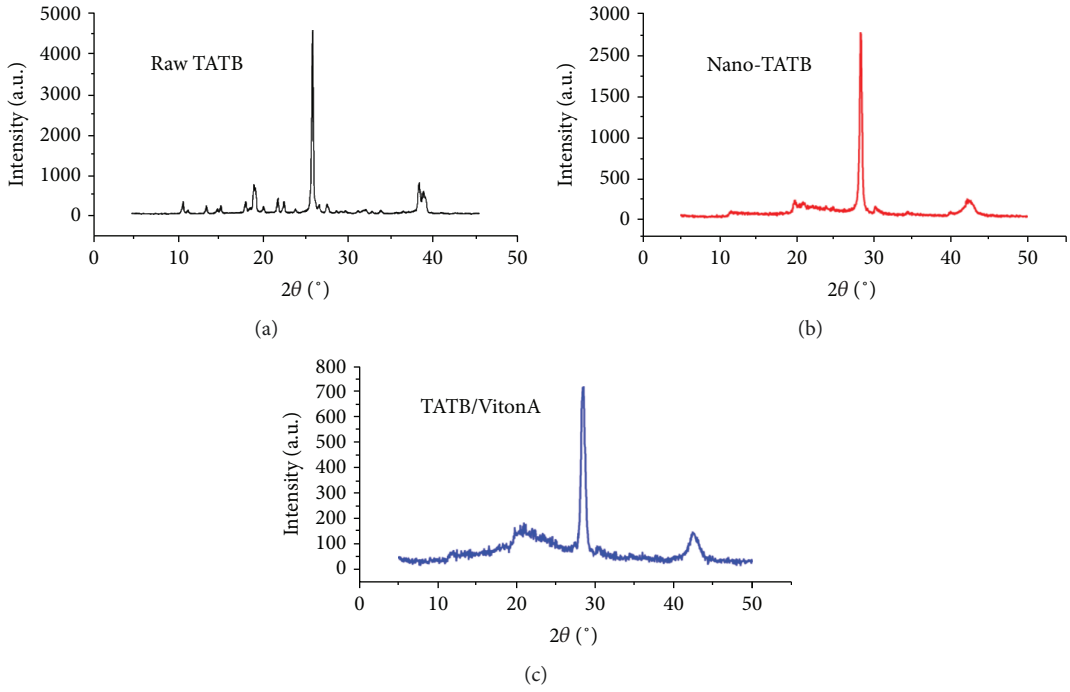

Figure 9: XRD patterns of raw TATB (a), nano-TATB (b), and TATB/VitonA nanocomposites (c).

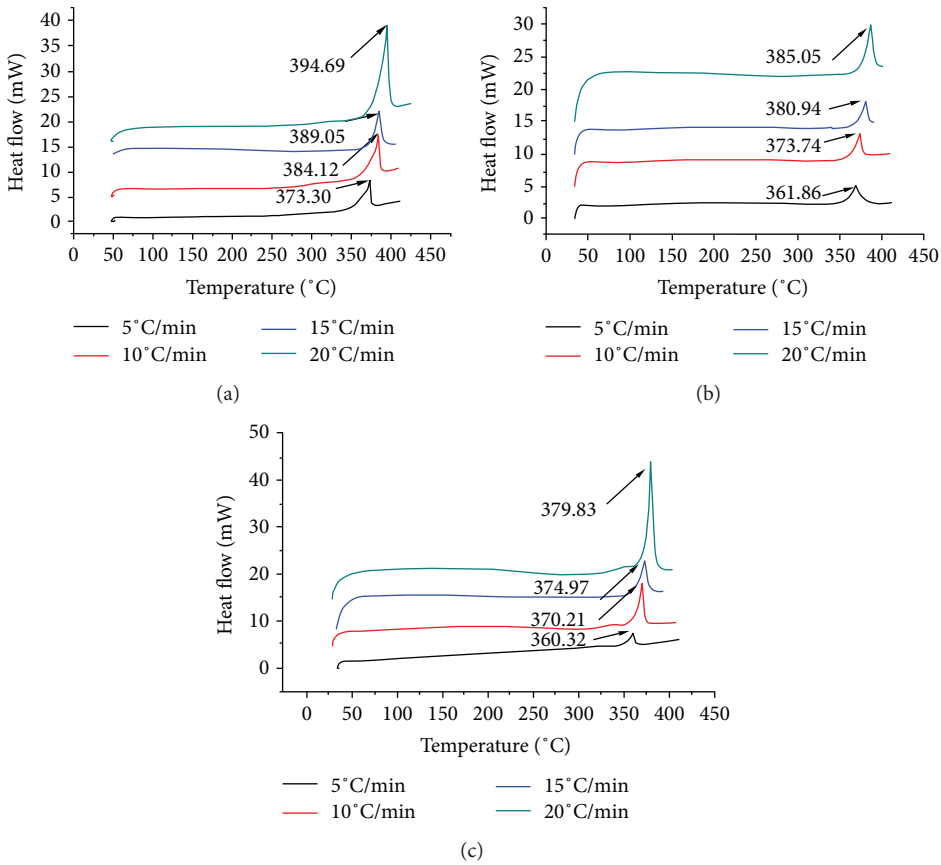

Figure 10: DSC diagram of raw TATB (a), nano-TATB (b), and TATB/VitonA nanocomposites (c) at different heating rates.

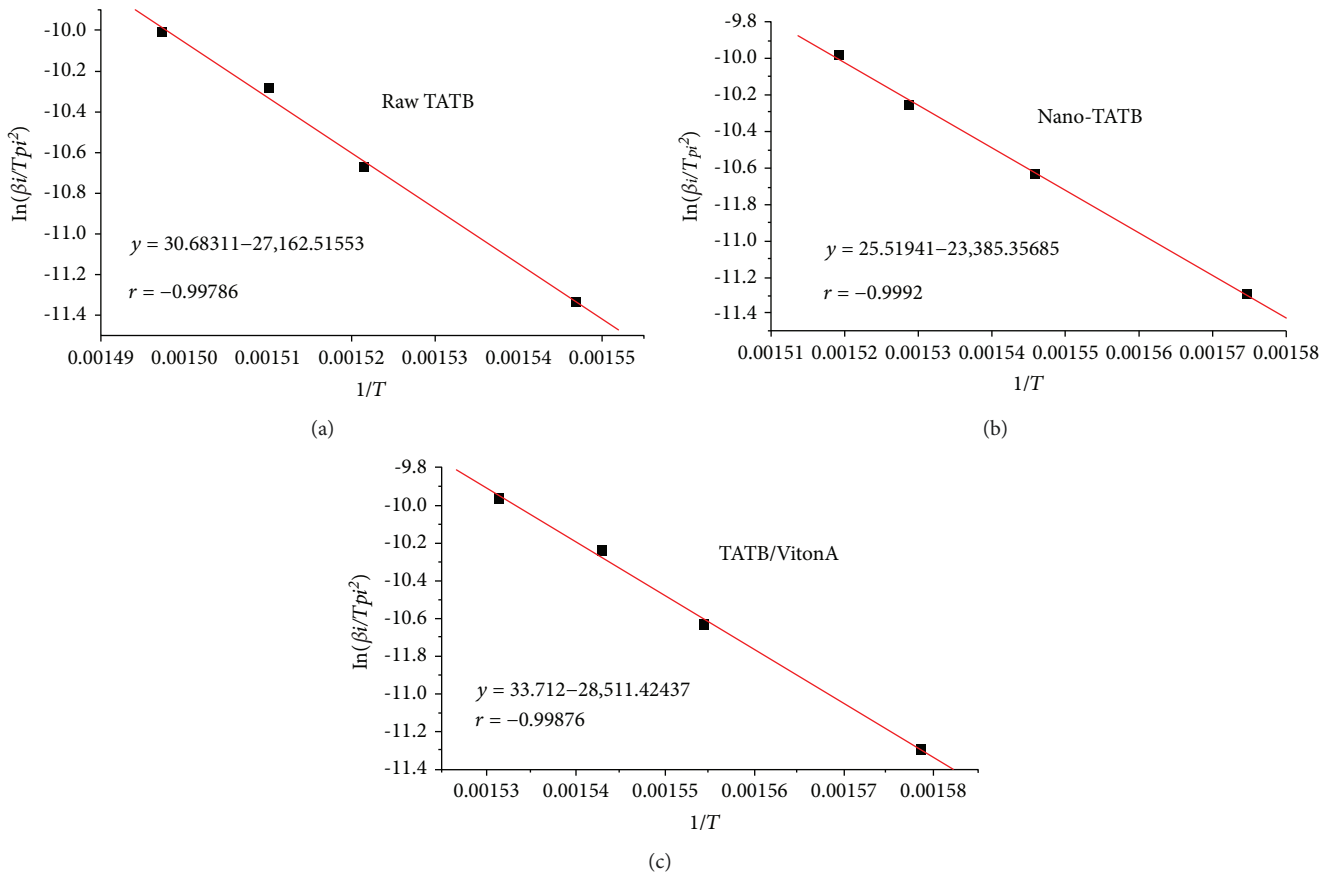

Figure 11: The Kissinger fitting lines of raw TATB (a), nano-TATB (b), and TATB/VitonA nanocomposites (c).

Table 1: Thermal decomposition kinetic parameters of TATB and TATB/VitonA nanocomposites.

Samples	E (kJ/mol)	A ($\min^{-1}$)	T_{p0} (°C)	T_b (°C)
Raw TATB	225.83	5.74×10^{17}	349.99	354.62
Nano-TATB	194.43	2.83×10^{16}	343.71	348.92
TATB/VitonA nanocomposites	237.05	1.25×10^{19}	340.07	344.23

with the increase of β heating rate. Their thermal decomposition apparent activation energy and preexponential factor were calculated by Kissinger's formula [24] and Rogers's method [25], respectively.

$$\ln \frac{\beta_i}{T_{pi}^2} = \ln \frac{AR}{E} - \frac{E}{RT_{pi}}, \qquad A = \frac{E\beta_i}{RT_{pi}^2} \exp\left(\frac{E}{RT_{pi}}\right), \tag{2}$$

where β_i is the heating rate ($\mathrm{K \cdot min^{-1}}$); T_{pi} is the decomposition peak temperature of the explosive at heating rate β_i; A is the preexponential factor ($\mathrm{min^{-1}}$); R is the gas constant ($8.314\ \mathrm{J \cdot mol^{-1} \cdot K^{-1}}$); and E is the apparent activation energy ($\mathrm{J \cdot mol^{-1}}$).

A straight line was obtained and shown in Figure 11 when $\ln(\beta_i/T_{pi}^2)$ was plotted against $1/T$. From the slope and the intercept of the straight line, the apparent activation energy and the preexponential factor could be calculated. The Kissinger fitting degree of the raw TATB, nano-TATB, and the TATB/VitonA nanocomposites were more than 99%, indicating that the measurement data was accurate and reliable.

According to the activation energy and preexponential factors of different materials, the critical temperature of the thermal explosion was calculated by formulas (3) and (4), respectively [26]. The calculation results are shown in Table 1.

$$T_{pi} = T_{p0} + b\beta_i + c\beta_i^2 + d\beta_i^3 \quad i = 1, 2, \ldots, 5, \tag{3}$$

$$T_b = \frac{E - \sqrt{E^2 - 4RET_{p0}}}{2R}. \tag{4}$$

It could be concluded (Table 1) that the thermal decomposition apparent activation energy and the thermal

Table 2: Detonation performances of TATB/VitonA nanocomposites.

Samples	Density (g/cm^3)	Pressure (GPa)	Temperature (K)	Velocity (m/s)
TATB/VitonA nanocomposites	1.646 (85%)	20.97	3073.95	7389.17
	1.743 (90%)	24.17	3026.03	7777.22
	1.840 (95%)	27.80	2969.78	8172.28

Table 3: Impact sensitivity of TATB and TATB/VitonA nanocomposites.

Samples	H_{50} [cm]	Standard deviation
Raw TATB	>150	0.047
Nano-TATB	112.5	0.062
TATB/VitonA nanocomposites	126.3	0.056

explosion critical temperature of the nano-TATB were lower than that of raw TATB. It was indicated that the specific surface area, heating area, and thermal conductivity of the explosive particles were increased, resulting in a decrease of activation energy and heat stability. The thermal decomposition apparent activation energy of TATB/VitonA nanocomposites was 237.05 kJ/mol, which was higher than that of raw TATB and nano-TATB. It could be concluded that the thermal stability of TATB/VitonA nanocomposites was the best.

3.6. Detonation Performances. The pressure density and detonation parameters of TATB/VitonA were calculated by the EXPLO5 program for evaluating its energetic properties. The detonation performance of the molding powder at a pressure density of 85%, 90%, and 95% of the theoretical density was shown in Table 2. As shown in Table 2, the detonation performance of TATB/VitonA bonded explosives varies with the pressure density. The higher the pressure density, the higher the detonation velocity and detonation pressure of the bonded explosive, and the lower the detonation temperature.

3.7. Impact Sensitivity. In order to study the safety performance of the sample, the test of the impact sensitivity was performed, and the results are shown in Table 3. The impact sensitivity of nano-TATB was higher than that of raw TATB. The main reason was the large contact area between nano-TATB explosive particles. During the impact process, the particle surface friction was fierce, which caused the hot spots to be more easily formed, and the result was the increased impact sensitivity. In contrast, the impact sensitivity of TATB/VitonA nanocomposites was lower than that of nano-TATB, indicating that the impact sensitivity of the nano-TATB coated with VitonA was reduced. The main reason was that the addition of VitonA could buffer some of the energy, and the energy acting on the nano-TATB particles was reduced, the less likely to cause energy accumulation and hot spots. Thus the possibility of impact detonation was reduced, and the impact sensitivity was decreased.

4. Conclusions

In this paper, nano-TATB was prepared by the ultrasonic-assisted spray method, and the TATB/VitonA nanocomposites were successfully prepared by the compressed air spray evaporation method based on nano-TATB. The TATB/VitonA nanocomposites consisted of spherical TATB particles 40–60 nm in size with a narrow particle size distribution of 0.5–1 μm. The crystal forms of the nano-TATB and TATB/VitonA nanocomposites and raw TATB were consistent, which indicated that the refinement and coating process did not change the crystal structure of TATB. From the results of thermal analysis, the thermal decomposition apparent activation energy of nano-TATB was slightly lower than that of raw TATB. The thermal decomposition apparent activation energy of TATB/VitonA nanocomposites was the highest, which was due to the high binding energy of VitonA and TATB. The apparent activation energy of TATB was increased due to the addition of VitonA. The detonation performance of TATB/VitonA nanocomposites varies with the pressure density. The impact sensitivity of nano-TATB was higher than that of raw TATB, and the impact sensitivity of TATB/VitonA nanocomposites was lower than that of nano-TATB.

Data Availability

The data used to support the findings of this study are available from the corresponding author upon request.

Conflicts of Interest

The authors declare that they have no conflicts of interest.

Acknowledgments

This research work was financially supported by the Advantage Disciplines Climbing Plan and Graduate Education Innovation Project of Shanxi Province.

References

[1] A. E. Gash, R. L. Simpson, and J. H. Satcher, "Energetic nanocomposites with sol-gel chemistry: synthesis, safety, and characterization," in *29th International Pyrotechnic Seminar*, pp. 1–15, Westminster, CO, USA, 2002.

[2] V. M. Boddu, D. S. Viswanath, T. K. Ghosh, and R. Damavarapu, "2,4,6-Triamino-1,3,5-trinitrobenzene (TATB) and TATB-based formulations—a review," *Journal of Hazardous Materials*, vol. 181, no. 1-3, pp. 1–8, 2010.

[3] D. M. Badgujar, M. B. Talawar, S. N. Asthana, and P. P. Mahulikar, "Advances in science and technology of modern

energetic materials: an overview," *Journal of Hazardous Materials*, vol. 151, no. 2-3, pp. 289–305, 2008.

[4] J. D. Yeager, A. M. Dattelbaum, E. B. Orler, D. F. Bahr, and D. M. Dattelbaum, "Adhesive properties of some fluoropolymer binders with the insensitive explosive 1,3,5-triamino-2,4,6-trinitrobenzene (TATB)," *Journal of Colloid and Interface Science*, vol. 352, no. 2, pp. 535–541, 2010.

[5] S. F. Rice and R. L. Simpson, *The Unusual Stability of TATB (1,3,5-Triamino-2,4,6-Trinitrobenzene): A Review of the Scientific Literature*, Tech. Rep. Lawrence Livermore National Lab, 1990.

[6] W. E. Voreck Jr., J. E. Brooks, J. R. Eberhardt, and H. A. Rezaie, "Shaped charge for a perforating gun having a main body of explosive including TATB and a sensitive primer," US Patent 5597974, 1997.

[7] C. M. Tarver, "Modeling detonation experiments on triaminotrinitrobenzene (TATB)-based explosives LX-17, PBX 9502, and ultrafine TATB," *Journal of Energetic Materials*, vol. 30, no. 3, pp. 220–251, 2012.

[8] M. B. Talawar, A. P. Agarwal, M. Anniyappan, G. M. Gore, S. N. Asthana, and S. Venugopalan, "Method for preparation of fine TATB (2-5 microm) and its evaluation in plastic bonded explosive (PBX) formulations," *Journal of Hazardous Materials*, vol. 137, no. 3, pp. 1848–1852, 2006.

[9] B. Gao, D. Wang, J. Zhang et al., "Facile, continuous and large-scale synthesis of CL-20/HMX nano co-crystals with high-performance by ultrasonic spray-assisted electrostatic adsorption method," *Journal of Materials Chemistry A*, vol. 2, no. 47, pp. 19969–19974, 2014.

[10] A. Elbeih, S. Zeman, M. Jungova, P. Vávra, and Z. Akstein, "Effect of different polymeric matrices on some properties of plastic bonded explosives," *Propellants, Explosives, Pyrotechnics*, vol. 37, no. 6, pp. 676–684, 2012.

[11] G. Yang, F. Nie, H. Huang, L. Zhao, and W. Pang, "Preparation and characterization of nano-TATB explosive," *Propellants, Explosives, Pyrotechnics*, vol. 31, no. 5, pp. 390–394, 2006.

[12] L. Yang, X. Ren, T. Li, S. Wang, and T. Zhang, "Preparation of ultrafine TATB and the technology for crystal morphology control," *Chinese Journal of Chemistry*, vol. 30, no. 2, pp. 293–298, 2012.

[13] X. L. Song, Y. Wang, L. X. Liu, C. W. An, J. Y. Wang, and J. L. Zhang, "Characterization of nano TATB fabricated by mechanical milling methodology," *Journal of Solid Rocket Technology*, vol. 40, no. 4, pp. 471–475, 2017.

[14] R. H. Gee, A. Maiti, and L. E. Fried, "Mesoscale modeling of irreversible volume growth in powders of anisotropic crystals," *Applied Physics Letters*, vol. 90, no. 25, article 254105, 2007.

[15] M. L. Hobbs and M. J. Kaneshige, "Ignition experiments and models of a plastic bonded explosive (PBX 9502)," *Journal of Chemical Physics*, vol. 140, no. 12, article 124203, 2014.

[16] A. P. Wemhoff, W. M. Howard, A. K. Burnham, and A. L. Nichols, "An LX-10 kinetic model calibrated using simulations of multiple small-scale thermal safety tests," *Journal of Physical Chemistry A*, vol. 112, no. 38, pp. 9005–9011, 2008.

[17] W. Ji, X. Li, J. Wang, B. Ye, and C. Wang, "Preparation and characterization of the solid spherical HMX/F2602 by the suspension spray-drying method," *Journal of Energetic Materials*, vol. 34, no. 4, pp. 357–367, 2016.

[18] X. Shi, J. Wang, X. Li, and C. An, "Preparation and characterization of HMX/Estane nanocomposites," *Central European Journal of Energetic Materials*, vol. 11, no. 3, pp. 433–442, 2014.

[19] X. Shi, J. Wang, X. Li, C. An, J. Wang, and W. Ji, "Preparation and properties of 1,3,5,7-tetranitro-1,3,5,7-tetrazocane-based nanocomposites," *Defence Science Journal*, vol. 65, no. 2, pp. 131–134, 2015.

[20] B. Y. Ye, C. W. An, J. Y. Wang, and X. H. Geng, "Formation and properties of HMX-based microspheres via spray drying," *RSC Advances*, vol. 7, no. 56, pp. 35411–35416, 2017.

[21] Z. Yang, J. Li, B. Huang, S. Liu, Z. Huang, and F. Nie, "Preparation and properties study of core-shell CL-20/TATB composites," *Propellants, Explosives, Pyrotechnics*, vol. 39, no. 1, pp. 51–58, 2014.

[22] A. K. Nandi, "Surface coating of cyclotetramethylenetetranitramine (HMX) crystals with the insensitive high explosive 1,3,5-triamino-2,4,6-trinitrobenzene (TATB)," *Central European Journal of Energetic Materials*, vol. 9, pp. 119–130, 2012.

[23] C. Lin, G. He, J. Liu et al., "Enhanced non-linear viscoelastic properties of TATB-based polymer bonded explosives filled with hybrid graphene/multiwalled carbon nanotubes," *RSC Advances*, vol. 5, no. 115, pp. 94759–94767, 2015.

[24] H. E. Kissinger, "Reaction kinetics in differential thermal analysis," *Analytical Chemistry*, vol. 29, no. 11, pp. 1702–1706, 1957.

[25] R. N. Rogers and G. W. Dauh, "Scanning calorimetric determination of vapor-phase kinetics data," *Analytical Chemistry*, vol. 45, no. 3, pp. 596–600, 2002.

[26] H. Wang, H. Zhang, R. Hu, E. Yao, and P. Guo, "Estimation of the critical rate of temperature rise for thermal explosion of nitrocellulose using non-isothermal DSC," *Journal of Thermal Analysis and Calorimetry*, vol. 115, no. 2, pp. 1099–1110, 2014.